Rational design of the nanostructure features on superhydrophobic surfaces for enhanced dynamic water repellency

Shen, Yizhou; Tao, Jie; Chen, Zhong; Zhu, Chunling; Wang, Guanyu; Chen, Haifeng; Liu, Senyun

2018

Shen, Y., Tao, J., Chen, Z., Zhu, C., Wang, G., Chen, H., & Liu, S. (2018). Rational design of the nanostructure features on superhydrophobic surfaces for enhanced dynamic water repellency. ACS Sustainable Chemistry and Engineering, 6(8), 9958-9965. doi:10.1021/acssuschemeng.8b01200

https://hdl.handle.net/10356/136726

https://doi.org/10.1021/acssuschemeng.8b01200

Rational design of the nanostructure features on superhydrophobic surfaces for enhanced dynamic water repellency

Yizhou Shen,[†,§] Jie Tao,[†,*] Zhong Chen,[§,*] Chunling Zhu,[†] Guanyu Wang,[†] Haifeng Chen,[‡] Senyun Liu[†]

[†] College of Materials Science and Technology, Nanjing University of Aeronautics and Astronautics, Nanjing 210016, P. R. China

[‡] Department of Materials Chemistry, Qiuzhen School, Huzhou University, 759, East 2nd Road, Huzhou 313000, P. R. China

[§] School of Materials Science and Engineering, Nanyang Technological University, Nanyang Avenue 50, Singapore 639798

KEYWORDS: dynamic water repellency; impact droplet; superhydrophobic surface; wetting interfaces

ABSTRACT: Biomimetic surfaces with various extents of liquid adhesion intensely appeal to many researchers due to their academic significance and potential industry applications. The present work aims to discuss the relationship between bouncing dynamics of impact droplets and static liquid adhesion driven by micro/-nanostructure features. Here we fabricated three types of nanostructure (nanotube, nanomesh, and nanowire) superhydrophobic surfaces based on the TiO_2 nano-materials, and all these resultant surfaces were endowed with the robust superhydrophobicity, and showed the low liquid adhesion with the sliding angles from 7.5° to 3°. Subsequently, the bouncing dynamics of impact droplets on these surfaces were evaluated and showed remarkable distinctions with different capacity to rebound off. This is explained that the impact droplet has induced a higher capillary-induced adhesion force interaction compared with the static droplet on nanotube structure surface due to the existence of dynamic pressure during the moving process. The produced high capillary-induced adhesion force interaction finally caused the impact droplet not bouncing off the surface. On the contrary, the impact droplet can successfully bounce off the nanowire structure surface, which is mainly due to the almost no capillary adhesion force interaction induced by the open structure system on the superhydrophobic surface.

1. INTRODUCTION

Materials that exhibit special wettability are of considerable significance, as witnessed by the rapid development over the past decades under the impetus of bionic manufacturing technologies.[1-4] To mimic biological functions, such as self-cleaning on lotus leaf surfaces, anti-fogging capacity of mosquito eyes, and some other features displayed by aquatic animals or plants, many efforts has been devoted to re-constructing these functional surfaces based on the synergistic action of surface rough structures and chemical compositions.[2,5-9] Superhydrophobic surfaces with the adjustable liquid adhesion have been a research focus, because of their potential applications in micro-fluidic device, robot, and aircraft anti-icing, *etc*. [10-14] The corresponding strategies are mainly to design the morphologies and sizes of microscopic structures for mediating the van der Waals and/or the capillary-induced adhesion force interactions between solid surface and liquid, finally realizing the purpose of regulating the liquid adhesion.[12,13,15]

On this basis, Zhao XD, *et al*. prepared various MnO_2 nanostructures and achieved superhydrophobicity with the apparent contact angle reaching 155°.[16] These nanostructures induced the different liquid adhesion from nearly 0 μN to 130 μN, which was explained from the view of kinetic barrier difference resulted from the unique extent of continuity of the triple-phase contact line. Subsequently, a large number of experimental investigations were reported to confirm and further enrich the studies on the regulation of water adhesion on superhydrophobic surfaces.[17,18] Liu K. *et al.* fabricated similar microscopic nanostructure polyimide films with the gecko's toes using anodic aluminum oxide (AAO) method.[19] The resultant surface possesses a high liquid adhesive force, showing the water droplet does not slide off the polyimide films when tilted at 90° or even 180°.

However, many recent studies indicate that the dynamics of impact droplets on solid surfaces are more practically meaningful and should be paid more attentions to.[20-23] It is of great interest to understand the condition of tuning the bouncing dynamics of impact droplets on solid surfaces of different microscopic features, and the correlation between static liquid adhesion and the corresponding bouncing dynamics of liquid droplets. In many practical situations, droplets would dynamically hit the surface at certain angle with a kinetic energy. Immediately after the droplet is in contact with a superhydrophobic surface, it spreads out to a maximal deformation and then retracts, before it finally bonces off the surface. As we know, the contact time of the entire impact process directly reflects the extent of energy transition between water droplet and surface, which is considered to be crucial to the anti-icing applications of superhydrophobic surfaces.[24,25] The contact time should be kept short enough to compel the supercooled droplets to rapidly rebound off before freezing. The aim of the present work is therefore to investigate the droplet bouncing dynamics on the nanostructure-designed superhydrophobic surfaces and to distinguish the dynamic interaction mechanisms.

Herein, three classes of superhydrophobic nanostructure surfaces were designed with nanotube, nanomesh, and nanowire (labelled as NT-Surface, NM-Surface, and NW-Surface, respectively).[26] As is well known, the surface nanostructures with lower surface free energy possess the capacity to allow the droplets to easily roll off or closely stick on the solid surfaces, and the underlying mechanism is that the nanostructures strongly affect the interface contact type between liquid and solid. As a dominant role of the interaction force at the interface, the capillary-induced adhesion force displays a great response to the change of contact type between liquid and solid, finally resulting in the variation of liquid adhesion on the nanostructure surfaces.[27,28] Obviously, the droplet bouncing dynamics can be reflected to a certain extent by the

liquid adhesion, yet some distinctions are also discovered that the viscous resistance against the moving direction is enhanced due to the existence of dynamic pressure F_D during the entire moving process of the dynamic impact droplet.[29-31] Consequently, the NT-Surface cannot compel impact droplets to bounce off, although it also has a lower liquid adhesion with a smaller sliding angle. With the change of nanostructures (NM-Surface and NW-Surface), the contact type between solid surface and water droplet gradually transforms to point-contact style with smaller surface fraction, finally leading to the gradually increased rebounding capacity of impact droplets. These findings will benefit the design of nanostructure surfaces for enhancing the droplet bouncing dynamics, and further deepening the understanding on the role of nanostructures behind these experimental phenomena, especially in the wetting aspect.

2. EXPERIMENTAL SECTION

2.1 Fabrication of three types of nanostructure superhydrophobic surfaces

The Ti6Al4V alloy plates (supplied by Baoji titanium industry Co., Ltd., China) were polished mechanically *via* metallographic abrasive paper (0#-6#) and cleaned ultrasonically in acetone, alcohol (analytical reagent, purchased from Aladdin Co., Ltd., China), and deionized water for 10 min, respectively. Following this, the pre-treated plates were constructed to form three types of designed nanostructures by means of different processing methods.

Nanotube structure (NT-Surface): Andox oxidation on the plate was carried out in the system of 0.5 wt % HF solution, and the plate was placed as working electrode. In this case, a constant voltage of 20 V was applied for 30 min at room environments. The as-prepared nanotube

structures was further treated with an annealing process to achieve the specific-crystal TiO_2 nanotube structures.

Nanomesh structure (NM-Surface): A two-step chemical etching method was used to produce the ideal nanomesh structures. Firstly, the cleaned plate was placed in the H_2SO_4 (40 wt%) solutoin to take place chemical reaction for 1 h at 65 °C. Subsequently, the pre-etching sample plate was neutralized by placing in a $NaHCO_3$ solution (0.1 M) for 5 min. The next step was to perform the alkaline etching in NaOH solution (3.5 M) at 65 °C with a reaction period of 18h to obtain the final nanomesh structure sample surface.

Nanowire structure (NW-Surface): For nanowire structure on the Ti alloy substrate, the cleaned sample plate occurred the hydrothermal reaction in 220 °C autoclave (containing 30 mL NaOH solution with 1 M concentration) for 8 h. At this time, the as-prepared nanowire structures was also neutralized by placing in 0.1 M HCl solution (0.5 h). Finally, the further annealing treatment was also needed to change the crystal form of TiO_2 nanowire arrays, and the main processing parameters were designed as 500 °C (2 °C/min to increase temperature) and 3 h.

To obtain the low surface energy for hydrophobicity, all these as-prepared nanostructures surfaces were immersed in a 1 wt% FAS-17 (1H,1H,2H,2H-perfluorooctyltriethoxysilane) ethanol solution. And after reacting with 24 h, these samples were dried in an 120 °C oven for 2 h to gain the final samples for appliation in the next experiments.

2.2 Characterizations of morphology and chemical composition

A field emission scanning electron microscopy (FE-SEM; Hitachi S4800, Japan) was used to observe the morphologies of the as-prepared nanostructures surfaces. The phase analyses on the nanostructures surfaces were performed by an X-ray diffractometry (UltimaIV, Rigaku Co., CuKα radiation, Japan), and the operating parameters were designed as 50 kV and 40 mA.

Furthermore, the chemical compositions of the nanostructures before and after FAS-17 modification were detected by an X-ray photoelectron spectrometer, Kratos AXIS UltraDLD, Japan.

2.3 Superhydrophobicity and dynamic water repellency

The superhydrophobicity were reflected by the apparent contact angle (APCA) and sliding angle (SA), which were measured by a contact angle analyzer (Kruss DSA100, Germany). During this measurement, a 4 μL reference water droplet was selected to characterize the superhydrophobicity, and average value was determined by three measurements. For dynamic water repellency, it was usually determined by contact time of impact droplet on solid surfaces. In this measurement, we used a high-speed camera (Photron Mini 100), each filming at 5,000 frames per second, to record the contact and movement process of impact droplet on the as-prepared nanostructures surfaces. To control the impact speed, the droplet was released from a height of 50 mm, so that the impact speed was 0.99 m/s.

3. RESULTS AND DISCUSSION

3.1 Design of the nanostructure surfaces

Figure 1 illustrates the schematic diagrams of three designed nanostructure models, and clearly depicts the contact ways between droplets and these nanostructure superhydrophobic surfaces. From a smooth substrate to the NW-Surface, the liquid/solid contact takes place a remarkable change with the reduced surface fraction. This mainly attributes to the quantity of air pockets entrapped in the nanostructures, which is also the basic requirement to produce

superhydrophobicity,[32,33] as a higher content of air pockets enhances water repellency. Furthermore, the morphologies of nanostructures also play an important role in improving the superhydrophobicity, especially reducing the liquid adhesion.

Y. Lai and his co-workers have demonstrated that the dominant capillary-induced adhesion force interaction depends on the sealed extent of trapped air pockets, which can be also easily tuned by changing the morphology feature and size of nanostructures.[32,34] The underlying principle is that nanostructure morphology features firstly determine whether the trapped air pockets can be effectively sealed in the nanostructures. If the situation of sealing the air pockets can take place, the size of nanostructures plays an important role in the control of sealed extent, fianlly realizing the purpose of regulating capillary-induced adhesion force interaction of liquid/solid. On this basis, the liquid ahesion on the solid surfaces can be easily controlled by means of designing the nanostructures with different morphology features and sizes. Following this, we designed and fabricated the NT-Surface, NM-Surface, and NW-Surface with the nanostructure morphology change from tube-shape to wire-shape. Among them, nanowire structures on the NW-Surface belong to the open-type topography and cannot seal the air pockets, yet the NT-Surface has the ability to seal the trapped air pockets and therefore induces a high liquid adhesion on the superhydrophobic surface. To obtain lower liquid adhesion, the diameter and length of nanotube structures were controlled to reduce the capillary adhesion force interaction of liquid/solid. In this work, the nanotube structures were prepared by means of anodic oxidation in the HF solution. The two main parameters of anodic oxidation voltage and time are used to control the geometric size of nanotube structures, and the corresponding morphologies of the as-prepared nanotube structures are shown in Figure S1 and Figure S2. As a consequence, the NT-Surface with the appropriate size and morphology can be endowed with the

almost same liquid adhesion with the other surfaces, *i.e.*, NM-Surface and NW-Surface. Subsequently, the bouncing dynamics of impact droplets on these surface were invesitgated (For the moving process of impact droplets, see Figure 1e and f), because the liquid adhesion might be re-increased to produce the influence on the moving process of impact droplet on the solid surface under the dynamic condition.

3.2 Static non-wettability derived from nanostructures and chemical compositions

The as-prepared sample surfaces exhibit the desired nanostructure morphologies and dimensions, which are depicted by the scanning electron microscope (SEM) images of Figure 2a-c. On the NT-Surface, the in-situ produced TiO_2 nanotube structures tidily and evenly distribute on the smooth substrate surface with the diameter of ~100 nm and length of ~200 nm. The density of surface nanotube structures is $\sim 6\times10^7$ /mm^2. Figure 2d shows the XRD patterns of the nanotube structures after the annealing treatment at different temperatures. The as-prepared amorphous nanotube is gradually transformed to the stable rutile phase TiO_2 with the increase of annealing temperatures.

The NM-Surface fabricated by chemical etching displays the uniform three-dimensional mesh nanostructures, and the crystal structure mainly consists of anatase phase TiO_2 (see Figure 2e). As illustrated in Figure 2b, the prepared three-dimensional mesh nanostructures have comparable dimensions with the NT-Surface, but the surface has a greater degree of three-dimensional openess. The increase in openness of nanostructures is further enlarged on the NW-Surface, which is fabricated by means of hydrothermal treatment (Figure 2c). The XRD patterns of the NW-Surface (Figure 2f) show the phase change at different experimental stages, and the final nanowire structures consist of anatase TiO_2 crystals. All three types of as-prepared TiO_2 nanostructures are further modified using the low energy fluocarbon material to achieve

superhydrophobicity, as shown in Figure S3. Figure 2g illustrates the X-ray photoelectron spectroscopy (XPS) spectrum of the as-prepared TiO_2 nanostructures before and after the surface modificaiton. It can be seen that the sample possesses high intensity peaks of the F1s and FKLL and low intensity peaks of the Ti2p and O1s after the modification. In high resolution spectrum of C1s (inset in Figure 2g), the peaks corresponding to $–CF_2$ (at 291 eV) and $–CF_3$ (at 294 eV) are observed, indicating that the low energy fluoroalkyl groups have been self-assembled onto the surfaces of as-prepared TiO_2 nanostructures. As a consequence, the three TiO_2 nanostructure surfaces have achieved the superhydrophobicity (insets in Figure 2a-c).

Nanostructures, as a determining factor, have the capacity to allow droplets to exhibit the different wetting states, and the detailed testing results of superhydrophobicity on the above three types of nanostructure surfaces are shown in Figure 2h and i. Obviously, all these nanostructure surfaces conform to the definition of superhydrophobic surface with the APCAs exceeding 150° and SAs less than 10°. Among them, the NW-Surface possesses a highest APCA up to 161° and the lowest SA of 3°, which is mainly due to the highest amount of air pockets entrapped by the structures. This is consistent with the analysis of the openness of the three types of nanostructures, and also can be well explained by the Cassie-Baxter wetting model.[35,36] Furthermore, the nanowire structures belong to the open structures that allow trapped air to flow easily underneath the droplets. The smaller surface fraction on the nanowire surface produces the lowest contact-line surface fraction (greatest discontinuity) of triple phases contact, finally leading to a low SA and liquid adhesion.[37] Note that the NT-Surface can still make the static droplets easily fall off at a SA of ~7.5°, which implies the capillary-induced adhesion force interaction still affects the liquid adhesion, but is not high enough to prevent the droplet from falling off the surface. Such phenomenon may be expected, because the nanotube structures seal

the air pockets and could produce larger adhesion force to the static droplets,[38,39] resulting in the droplets falling off at a SA of ~7.5°. It should be noted that the wetting parameters of the smooth substrate without any treatments, and the contact angle is approximately 78°, and the SA cannot be tested owing to the higher liquid adhesion force. The corresponding SEM image of the smooth substrate is also shown in Figure S4.

3.3 Dynamic bahaviors of impact droplets

The dynamic processes of water droplets impacting on these nanostructured superhydrophobic surfaces exhibit a remarkable distinct behavior. Figure 3 shows the dynamic processes of water droplets impacting on the sample surfaces with the impact velocity of ~1 m/s and the initial droplet diameter of 2 mm (For more details, please see supporting video). Although the NT-Surface also displays robust water repellency, impact droplet cannot successfully bounce off, as the impact droplet on the untreated smooth substrate does. This implies that the dominant capillary-induced adhesion force interaction between liquid and NT-Surface is further increased during the dynamic moving process, inducing a high viscous resistance against detachment of the impact droplets.[40]

With the change of openness on the NM-Surface, the droplet bouncing dynamics show an obvious improvement with the impact droplet successfully detached from the surface after 19 ms in spite of a loath separation. Also, the droplet was divided into two small droplets after the detachment due to the viscous resistance. On the NW-Surface, however, the impact droplet can agilely rebound off without any stagnancy, resulting from the extremely low capillary-induced adhesion force interaction induced by the high openness of nanowire structures. Overall, the impact droplets on the above three types of nanostructure surfaces will firstly spread to the

maximum deformation, and then starts to retract. Also, the spreading processes with the time of 2.2 ms show no distinctions among the three nanostructured surfaces, so that the displayed difference of droplet bouncing dynamics mainly depends on the retracting processes.

Figure 4a plots the variation of wetting position of impact droplets on the three nanostructure surfaces and the untreated substrate with the time. The wetting position is represented by D/D_0 (D is the diameter of contact area of impact droplet with solid surface, and $D_0 \approx 2$ mm is the initial diameter of droplet). Clearly, all these impact droplets reach their maximum deformation diameter (D_{max}) at 2.2 ms, indicating that the influence of nanostructures on spreading process to the maximum deformation is not significant due to the shorter period of energy conversion between initial kinetic energy and surface energy.[41-43] This further demonstrates that the final difference of droplet bouncing dynamics depends on the subsequent retracting process, as reflected in Figure 4a. The wetting positions (D/D_0) of impact droplets on the smooth Substrate and NT-Surface gradually tends toward stability at the levels of 1.5 and 0.7 after 13 ms, yet those on the NM-Surface and NW-Surface can successfully reduce to zero at 19 ms and 12.4 ms, respectively.

3.4 Topography-dependent dynamic behaviors

To more intuitively reflect the droplet bouncing dynamics on these nanostructure surfaces, we derived the function curve of the rate of wetting positions (D/D_0) with the time, as shown in Figure 4b. As descripte above, the remarkable distinction lies with the retracting process, where the retracting rate of wetting position on the NW-Surface is markedly higher than those on the other solid surfaces (*i.e.*, smooth Substrate, NT-Surface, and NM-Surface). Also, the NT-Surface only shows a slightly greater droplet bouncing capacity than Substrate and is lower than the NM-Surface. Meanwhile, the representative images (Figure 4c) selected from the retracting processes

at the same moment (at 5.8 ms) can also reveal the similar tendency of droplet bouncing dynamics on the above three nanostructure surfaces. It can be concluded that different types of nanostructures on the superhydrophobic surfaces can induce almost equivalent water repellency (for static droplets), however the dynamic droplet bouncing behavior exhibits great differences.

Essentially, wetting hysteresis is defined by the moving capacity of droplets on solid surfaces, and represented by the difference of advancing contact angle θ_{A} and receding contact angle θ_{R}. Generally, the hysterisis can be measured by the change of contact line position under the condition of adding and retracting liquid droplet on solid surface. This implies that there is a force to be induced to prevent the moving of contact line, *i.e.*, wetting hysteresis tension (f_A, f_R). According to the mechanics balance condition, the following equations can be derived:

$$\cos\theta_A = \frac{\sigma_{sg} - \sigma_{sl}}{\sigma_{\mathrm{lg}}} - \frac{f_A}{\sigma_{\mathrm{lg}}} = \cos\theta - \frac{f_A}{\sigma_{\mathrm{lg}}} \tag{1}$$

$$\cos\theta_R = \frac{\sigma_{sg} - \sigma_{sl}}{\sigma_{\mathrm{lg}}} - \frac{f_R}{\sigma_{\mathrm{lg}}} = \cos\theta - \frac{f_R}{\sigma_{\mathrm{lg}}} \tag{2}$$

where σ_{sg}, σ_{sl}, and σ_{lg}, are the interfacial tensions of solid-gas, solid-liquid and liquid-gas, respectively. As mentioned above, the moving of impact droplet on solid surface spreads to the maximum defromation at advancing contact angle θ_{A} and retracts at receding contact angle θ_{R} until the droplet bounces off the surface. Furthermore, the wetting hysteresis depends on the capillary adhesion force interaction between liquid and solid surface. Thus, the dynamic moving process of impact droplet on the solid surface is mainly determined by the wetting hysteresis, which has an intensely dependent relationship on the capillary-induced adhesion force interaction between liquid and solid surface. Here the values of advancing and receding contact angles are listed in the Table S1 in Supporting Materials.

At this point, it can be reasonably argued that the capillary force interaction becomes higher due to the existence of dynamic pressure during the moving process of impact droplet on the NT-Surface. The contact interface details of impact droplet on the NT-Surface (see Figure 4d and f) suggest that the liquid level permeating into the nanotube structures with higher degree comparing with the static droplets, and during the retracting stage the permeated liquid level will induce higher negative-pressure action Δf (as marked by the red lines in Figure 4f), which implies stronger capillary force interaction to prevent the impact droplets from bouncing off. The increasing curvature will produce a higher capillary-induced adhesion force interaction, and the relationship can be reflected by relation $\Delta f \propto k\sigma\rho$, where σ and ρ are surface tension and the curvature of liquid level, respectively.[44,45] As a consequence, the high curvature of liquid level in nanotube induces a strong capillary adhesion force to finally prevent the motion of the impact droplet on the NT-Surface, leading to the impact droplet not able to bounce off.

When the static droplet is placed on the NT-Surface, the liquid level permeating into the nanotube is almost flat. Therefore, the resultant capillary-induced adhesion force interaction cannot hinder the droplet from sliding off. Thus, the NT-Surface, which possesses the superhydrophobicity with the APCA exceeding 150° and a small SA of ~7.5°, cannot compel the impact droplet to bounce off. For the NW-Surface, there is almost no capillary adhesion force interaction between liquid and solid surface due to the flowing air entrapped by the open structures system on the superhydrophobic surface (see Figure 4e and g). Furthermore, comparing with NT-Surface, NW-Surface has smaller actual contact area of solid/liquid (whether static or dynamic wetting state), resulting in lower Vander Waals force. Therefore, the NW-Surface displays the robust superhydrophobicity (APCA reaching 161° and SA lowing to 3°), and simultaneously possesses a great capacity to compel impact droplet to rapidly bounce off.

4. CONCLUSION

In summary, we designed and fabricated three types of nanostructure superhydrophobic surfaces based on the TiO_2 nano-materials. All these resultant surfaces were endowed with the robust superhydrophobicity, and showed the low liquid adhesion with the sliding angles from 7.5° to 3°. However, the remarkable distinctions of bouncing dynamics of impact droplets on these nanostructure surfaces were revealed that impact droplet induced a higher capillary-induced interaction comparing with the static droplet on nanotube structure surface due to the existence of dynamic pressure during the moving process. The produced high capillary interaction finally caused the impact droplet not bouncing off the surface. On the opposite, the impact droplet can successfully bounce off the nanowire structure surface, which is mainly attributed to the almost no capillary interaction by its open structure system. These findings are useful to understand dynamic wetting behaviors of impact droplets on the solid surfaces, and guide the rational design of nanostructures for the tunable droplet bouncing capacity.

Supporting Information

AUTHOR INFORMATION

Corresponding Author

* Professor Jie Tao, Tel/Fax: +86-25-5211 2911. E-mail: taojie@nuaa.edu.cn.Pro

Professor Zhong Chen, Tel: +65 6790 4256. E-mail: ASZChen@ntu.edu.sg

Present Addresses

† College of Materials Science and Technology, Nanjing University of Aeronautics and Astronautics, Nanjing 210016, P. R. China

‡ Department of Materials Chemistry, Qiuzhen School, Huzhou University, 759, East 2nd Road, Huzhou 313000, P. R. China

§ School of Materials Science and Engineering, Nanyang Technological University, Nanyang Avenue 50, Singapore 639798

Notes

The authors declare no competing financial interest.

ACKNOWLEDGMENTS

J.T. acknowledges the support of the National Natural Science Foundation of China (No. 51671105 and No. 51705244). Y.S. and G.W. acknowledge the support of the Natural Science Foundation of Jiangsu Province (No. BK20170790), the Project Funded by China Postdoctoral Science Foundation (2017M610329), Jiangsu Planned Projects for Postdoctoral Research Funds (No. 1701145B), and A Project Funded by the Priority Academic Program Development of Jiangsu Higher Education Institutions. H.C. acknowledges the financial support of the General Project of Zhejiang Provincial Department of Education (No. Y201737320).

REFERENCES

(1) a) Li, S.; Huang, J.; Chen, Z.; Chen, G.; Lai, Y. A review on special wettability textiles: theoretical models, fabrication technologies and multifunctional applications. *J. Mater. Chem. A* **2017**, 5, 31-55; b) Cao, M.; Guo, D.; Yu, C.; Li, K.; Liu, M.; Jiang, L. Water-repellent properties of superhydrophobic and lubricant-infused "Slippery" surfaces: A brief study on the functions and applications. *ACS Appl. Mater. Interfaces* **2016**, 8, 3615-3623.

(2) a) Manna, U.; Lynn, D. M. Synthetic surfaces with robust and tunable underwater superoleophobicity. *Adv. Fun. Mater.* 2015, 25, 1672-1681.; b) Yao, X.; Song, Y.; Jiang, L. Applications of bio-inspired special wettable surfaces. *Adv. Mater.* **2011**, 23, 719-734.; c) Cao, M.; Jin, X.; Peng, Y.; Yu, C.; Li, K.; Liu, K.; Jiang, L. Unidirectional wetting properties on multi-bioinspired magnetocontrollable slippery microcilia. *Adv. Mater.* **2017**, 29, 1606869.

(3) a) Luo, Y.; Li, J.; Zhu, J.; Zhao, Y.; Gao, X. Fabrication of condensate microdrop self-propelling porous films of cerium oxide nanoparticles on copper surfaces. *Angew. Chem. Int. Ed.* **2015**, 54, 4876-4879.; b) Tian, D.; Song, Y.; Jiang, L. Patterning of controllable surface wettability for printing techniques. *Chem. Soc. Rev.* **2013**, 42, 5184-5209.; c) Kuang, M.; Wang, J.; Jiang, L. Bio-inspired photonic crystals with superwettability. *Chem. Soc. Rev.* **2016**, 45, 6833-6854.

(4) a) Berger, S.; Lonov, L.; Synytska, A. Engineering of ultra-hydrophobic functional coatings using controlled aggregation of bicomponent core/shell janus particles. *Adv. Fun. Mater.* **2011**, 21, 2338-2344.; b) Wang, B.; Liang, W.; Guo; Z.; Liu, W. Biomimetic super-lyophobic and super-lyophilic materials applied for oil/water separation: a new strategy beyond nature. *Chem. Soc. Rev.* **2015**, 44, 336-361.; c) Jiang, C.; Wang, Q.; Wang, T. Tunable wettability via counterion exchange of polyelectrolyte brushes grafted on cotton fabric. *New J. Chem.* **2012**, 36, 1641-1645.

(5) a) Zhang, L.; Dillert, R.; Bahnemann, D.; Vormoor, M. Photo-induced hydrophilicity and self-cleaning: models and reality. *Energy Environ. Sci.* **2012**, 5, 7491-7507.; b) Ragesh, P.; Ganesh, V. A.; Nair, S. V.; Nair, A. S. A review on 'self-cleaning and multifunctional materials'. *J. Mater. Chem. A* **2014**, 2, 14773-14797.

(6) Sun, Z.; Liao, T.; Liu, K.; Jiang, L.; Kim, J. H.; Dou, S. X. Fly-eye inspired superhydrophobic anti-fogging inorganic nanostructures. *Small* **2014**, 10, 3001-3006.

(7) a) Cai, Y.; Lin, L.; Xue, Z.; Liu, M.; Wang, S.; Jiang, L. Filefish-inspired surface design for anisotropic underwater oleophobicity. *Adv. Fun. Mater.* **2014**, 24, 809-816.; b) Chae, S. S.; Kim, K. H.; Park, J. H.; Lee, K. H.; Han, S. W.; Oh, J. Y.; Baik, H. K.; Kim, Y. S. Ultrathin photo-oxidized siloxane layer for extreme wettability: Anti-fogging layer for spectacles. *Adv. Mater. Interfaces* **2016**, 3, 1500725.

(8) Li, L.; Li, B.; Dong, J.; Zhang, J. Roles of silanes and silicones in forming superhydrophobic and superoleophobic materials. *J. Mater. Chem. A* **2016**, 4, 13677-13725.

(9) a) Si, Y. Guo, Z. Superhydrophobic nanocoatings: from materials to fabrications and to applications. *Nanoscale* **2015**, 7, 5922-5946.; b) Zhang, X.; Shi, F.; Niu, J.; Jiang, Y.; Wang, Z. Superhydrophobic surfaces: from structural control to functional application. *J. Mater. Chem.* **2008**, 18, 621-633.; c) Verho, T.; Bower, C.; Andrew, P.; Franssila, S.; Ikkala, O.; Ras, R. H. A. Mechanically durable superhydrophobic surfaces. *Adv. Mater.* **2011**, 23, 673-678.

(10) a) Peyer, K. E.; Zhang, L.; Nelson, B. J. Bio-inspired magnetic swimming microrobots for biomedical applications. *Nanoscale* **2013**, 5, 1259-1272.; b) Deng, N.; Sun, J.; Wang, W.; Ju, X.; Xie, R.; Chu, L. Wetting-induced coalescence of nanoliter drops as microreactors in microfluidics. *ACS Appl. Mater. Interfaces* **2014**, 6, 3817-3821.

(11) a) Cadirov, N.; Booth, J. A.; Turner, K. L.; Israelachvili, J. N. Influence of humidity on grip and release adhesion mechanisms for gecko-inspired microfibrillar surfaces. *ACS Appl. Mater. Interfaces* **2017**, 9, 14497-14505.; b) Sethi, S.; Ge, L.; Ci, L.; Ajayan, P. M.; Dhinojwala, A. Gecko-inspired carbon nanotube-based self-cleaning adhesives. *Nano Lett.* **2008**, 8, 822-825.

(12) Lv, J.; Song,Y.; Jiang, L.; Wang, J. Bio-inspired strategies for anti-icing. *ACS Nano* **2014**, 8, 3152-3169.

(13) a) Zhang, J.; Gu, C.; Tu, J. Robust slippery coating with superior corrosion resistance and anti-icing performance for AZ31B Mg alloy protection. *ACS Appl. Mater. Interfaces* **2017**, 9, 11247-11257.; b) Kirillova, A.; Ionov, L.; Roisman, I. V.; Synytska, A. Hybrid hairy janus particles for anti-icing and de-icing surfaces: Synergism of properties and effects. *Chem. Mater.* **2016**, 28, 6995-7005.; c) Shen, Y.; Tao, J.; Tao, H.; Chen, S.; Pan, L.; Wang, T. Anti-icing

potential of superhydrophobic Ti6Al4V surfaces: Ice nucleation and growth. *Langmuir* **2015**, 31, 10799-10806.

(14) Sun, X.; Damle, V. G.; Liu, S.; Rykaczewski, K. Bioinspired stimuli-responsive and antifreeze-secreting anti-icing coatings. *Adv. Mater. Interfaces* **2015**, 2, 1400479.

(15) a) Tadmor, R.; Das, R.; Gulec, S.; Liu, J.; N'guessan, H. E.; Shah, M.; Wasnik, P. S.; Yadav, S. B. Solid-liquid work of adhesion. *Langmuir* **2017**, 33, 3594-3600.; b) Kim, D.; Seo, J.; Shin, S.; Lee, S.; Lee, K.; Cho, H.; Shim, W.; Lee, H.; Lee, T. Reversible liquid adhesion switching of superamphiphobic Pd-decorated Ag dendrites via gas-induced structural changes. *Chem. Mater.* **2015**, 27, 4964-4971.

(16) Zhao, X. D., Fan, H. M., Liu, X. Y., Pan, H., Xu, H. Y. Pattern-dependent tunable adhesion of superhydrophobic MnO_2 nanostructured film. *Langmuir* **2011**, 27, 3224-3228.

(17) Huber, G., Mantz, H., Spolenak, R., Mecke, K., Jacobs, K., Gorb, S.N., et al. Evidence for capillarity contributions to gecko adhesion from single spatula nanomechanical measurements. *P. Natl. Acad. Sci. USA* **2005**, 102, 16293-16296.

(18) Lai, Y., Lin, C., Huang, J., Zhuang, H., Sun, L., Nguyen, T. Markedly controllable adhesion of superhydrophobic spongelike nanostructure TiO_2 films. *Langmuir* 2008, 24, 3867-3873.

(19) Liu, K., Du, J., Wu, J., Jiang, L. Superhydrophobic gecko feet with high adhesive forces toward water and their bio-inspired materials. *Nanoscale* **2012**, 4, 768-772.

(20) Mertaniemi, H.; Forchheimer, R.; Ikkala, O.; Ras, R. H. A. Rebounding droplet-droplet collisions on superhydrophobic surfaces: From the phenomenon to droplet logic. *Adv. Mater.* **2012**, 24, 5738-5743.

(21) Liang, Y.; Peng, J.; Li, X.; Xu, J.; Zhang, Z.; Ren, L. From natural to biomimetic: The superhydrophobicity and the contact time. *Microsc. Res. Tech.* **2016**, 79, 712-720.

(22) a) Zhang, R.; Hao, P.; He, F. Rapid bouncing of high-speed drops on hydrophobic surfaces with microcavities. *Langmuir* **2016**, 32, 9967-9974.; b) Zhao, B.; Wang, X.; Zhang, K.; Chen, L.; Deng, X. Impact of viscous droplets on superamphiphobic surfaces. *Langmuir* **2017**, 33, 144-151.

(23) a) Li, J.; Hou, Y.; Liu, Y.; Hao, C.; Li, M.; Chaudhury, M. K.; Yao, S.; Wang, Z. *Nat. Phys.* Directional transport of high-temperature Janus droplets mediated by structural topography. **2016**,

12, 606-612.; b) Liu, Y.; Moevius, L.; Xu, X.; Qian, T.; Yeomans, J. M.; Wang, Z. *Nat. Phys.* Pancake bouncing on superhydrophobic surfaces. **2014**, 10, 515-519.; c) Ruiter, J.; Lagraauw, R.; Ende, D.; Mugele, F. Wettability-independent bouncing on flat surfaces mediated by thin air films. *Nat. Phys.* **2015**, 11, 48-53.

(24) Shen, Y., Tao. J., Tao, H., Chen, S., Pan, L., Wang, T. Approaching the theoretical contact time of a bouncing droplet on the rational macrostructured superhydrophobic surfaces. *Appl. Phys. Lett.* **2015**, 107, 111604.

(25) Richard, D., Clanet, C., Quéré, D. Surface phenomena: Contact time of a bouncing drop. *Nature* **2002**, 417, 811.

(26) a) Huang, J.; Lai, Y.; Wang, L.; Li, S.; Ge, M.; Zhang, K.; Fuchs, H.; Chi, L. Controllable wettability and adhesion on bioinspired multifunctional TiO_2 nanostructure surfaces for liquid manipulation. *J. Mater. Chem. A* **2014**, 2, 18531-1858-38.; b) Klittich, M. R.; Wilson, M. C.; Bernard, C.; Rodrigo, R. M.; Keith, A. J.; Niewiarowski, P. H.; Dhinojwala, A. Influence of substrate modulus on gecko adhesion. *Sci. Rep.* **2017**, 7, 43647.

(27) a) You, S.; Wan, M. P. Mathematical models for the van der Waals force and capillary force between a rough particle and surface. *Langmuir* **2013**, 29, 9104-9117.; b) Davies, G. B.; Krüger, T.; Coveney, P. V.; Harting, J.; Bresme, F. Assembling ellipsoidal particles at fluid interfaces using switchable dipolar capillary interactions. *Adv. Mater.* **2014**, 26, 6715-6719.

(28) Danov, K. D.; Stanimirova, R. D.; Kralchevsky, P. A.; Marinova, K. G.; Stoyanov, S. D.; Blijdenstein, T. B. J.; Cox, A. R.; Pelan, E. G. Adhesion of bubbles and drops to solid surfaces, and anisotropic surface tensions studied by capillary meniscus dynamometry. *Adv. Colloid Interfac.* **2016**, 233, 223-239.

(29) Ellinas, K.; Chatzipetrou, M.; Zergioti, I.; Tserepi, A.; Gogolides, E. Superamphiphobic polymeric surfaces sustaining ultrahigh impact pressures of aqueous high- and low-surface-tension mixtures, tested with laser-induced forward transfer of drops. *Adv. Mater.* **2015**, 27, 2231-2235.

(20) a) Checco, A.; Rahman, A.; Black, C. T. Robust superhydrophobicity in large-area nanostructured surfaces defined by block-copolymer self assembly. *Adv. Mater.* **2014**, 26, 886-

891.; b) Lee, C.; Nam, Y.; Lastakowski, H.; Hur, J. I.; Shin, S.; Biance, A.; Pirat, C.; Kim, C.; Ybert, C. *Soft Matter* **2015**, 11, 4592-4599.

(31) a) Singh, E.; Chen, Z.; Houshmand, F.; Ren, W.; Peles, Y.; Cheng, H.; Koratkar, N. Superhydrophobic graphene foams. *Small* **2013**, 9, 75-80.; b) Zhu, L.; Shi, P.; Xue, J.; Wang, Y.; Chen, Q.; Ding, J.; Wang, Q. Superhydrophobic stability of nanotube array surfaces under impact and static forces. *ACS Appl. Mater. Interfaces* **2014**, 6, 8073-8079.

(32) a) Wang, T.; Cui, J.; Ouyang, S.; Cui, W.; Wang, S. A new approach to understand the Cassie state of liquids on superamphiphobic materials. *Nanoscale* **2016**, 8, 3031-3039.; b) Ramachandran, R.; Nosonovsky, M. Coupling of surface energy with electric potential makes superhydrophobic surfaces corrosion-resistant. *Phys. Chem. Chem. Phys.* **2015**, 17, 24988-24997.

(33) Zhu, H.; Guo, Z.; Liu, W. Biomimetic water-collecting materials inspired by nature. *Chem. Commun.* **2016**, 52, 3863-3879.

(34) a) Lai, Y.; Gao, X.; Zhang, H.; Huang, J.; Lin, C.; Jiang, L. Designing superhydrophobic porous nanostructures with tunable water adhesion. *Adv. Mater.* **2009**, 21, 3799-3803.; b) Lai, Y.; Lin, C.; Huang, J.; Zhang, H.; Sun, L.; Nguyen, T. Markedly Controllable adhesion of superhydrophobic spongelike nanostructure TiO_2 films. *Langmuir* **2008**, 24, 3867-3873.

(35) Hejazi, V.; Moghadam, A. D.; Rohatgi, P.; Nosonovsky, M. Beyond Wenzel and Cassie–Baxter: Second-order effects on the wetting of rough surfaces. *Langmuir* **2014**, 30, 9423-9429.

(36) Kaufman, Y.; Chen, S.; Mishra, H.; Schrader, A. M.; Lee, D. W.; Das, S.; DonaldsonJr, S. H.; Israelachvili, J. N. Simple-to-apply wetting model to predict thermodynamically stable and metastable contact angles on textured/rough/patterned surfaces. *J. Phys. Chem. C* **2017**, 121, 5642-5656.

(37) a) Erbil, H. Y. The debate on the dependence of apparent contact angles on drop contact area or three-phase contact line: A review. *Surf. Sci. Rep.* **2014**, 69, 325-365.; b) Guo, T.; Li, M.; Heng, L.; Jiang, L. Special adhesion of natural honeycomb walls and their application. *Phys. Chem. Chem. Phys.*, **2015**, 17, 6242-6247.; c) Pittoni, P. G.; Tsao, H.; Hung, Y.; Huang, J.; Lin, S. Impingement dynamics of water drops onto four graphite morphologies: From triple line recoil to pinning. *J. Colloid Interf. Sci.* **2014**, 417, 256-263.

(38) Hu, Z.; Zhang, X.; Liu, Z.; Huo, K.; Chu, P. K.; Zhai, J.; Jiang, L. Regulating water adhesion on superhydrophobic TiO_2 nanotube arrays. *Adv. Fun. Mater.* **2014**, 24, 6381-6388.

(39) Chen, B.; Zhang, G.; Oppenheimer, P. G.; Zhang, C.; Tornatzky, H.; Esconjauregui, S.; Hofmann, S.; Robertson, J. Influence of packing density and surface roughness of vertically-aligned carbon nanotubes on adhesive properties of gecko-inspired mimetics. *ACS Appl. Mater. Interfaces* **2015**, 7, 3626-3632.

(40) a) Kim, J.; Rothstein, J. P. Droplet impact dynamics on lubricant-infused superhydrophobic surfaces: The role of viscosity ratio. *Langmuir* **2016**, 32, 10166-10176.; b) Mitra, S.; Sathe, M. J.; Doroodchi, E.; Utikar, R.; Shah, M. K.; Pareek, V.; Joshi, J. B.; Evans, G. M. Droplet impact dynamics on a spherical particle. *Chem. Eng. Sci.* **2013**, 100, 105-119.

(41) Oberli, L.; Caruso, D.; Hall, C.; Fabretto, M.; Murphy, P. J.; Evans, D. Condensation and freezing of droplets on superhydrophobic surfaces. *Adv. Colloid, Interfaces* **2014**, 210, 47-57.

(42) Lu, Y.; Sathasivam, S.; Song, J.; Xu, W.; Carmalt, C. J.; Parkin, I. P. Water droplets bouncing on superhydrophobic soft porous materials. *J. Mater. Chem. A* **2014**, 2, 12177-12184.

(43) a) Bird, J. C.; Dhiman, R.; Kwon, H.; Varanasi, K. K. Reducing the contact time of a bouncing drop. *Nature* **2013**, 503, 385-388.; b) Schutzius, T. M.; Graeber, G.; Elsharkawy, M.; Oreluk, J.; Megaridis, C. M. Morphing and vectoring impacting droplets by means of wettability-engineered surfaces. *Sci. Rep.* **2013**, 4, 7029.

(44) Ershov, D.; Sprakel, J.; Appel, J.; Stuart, M. A. C.; Gucht, J. *P.* Capillarity-induced ordering of spherical colloids on an interface with anisotropic curvature. *Natl. Acad. Sci. USA* **2013**, 110, 9220-9224.

(45) a) Park, B. J.; Lee, M.; Lee, B.; Furst, E. M. Lateral capillary interactions between colloids beneath an oil–water interface that are driven by out-of-plane electrostatic double-layer interactions. *Soft Matter* **2015**, 11, 8701-8706.; b) Ye, M.; Deng, X.; Ally, J.; Papadopoulos, P.; Schellenberger, F.; Vollmer, D.; Kappl, M.; Butt, H. Superamphiphobic particles: How small can we go? *Phys. Rev. Lett.* **2014**, 112, 016101.

TOC Graphic:

Different from nanowire structure surface with a complete open system, impact droplet induced a higher capillary-induced adhesion force interaction on the nanotube structure surface under the condition of dynamic pressure. The produced high capillary adhesion force interaction prevented the impact droplets to bounce off, and the capillary force can be tuned by the open extent of nanostructures.

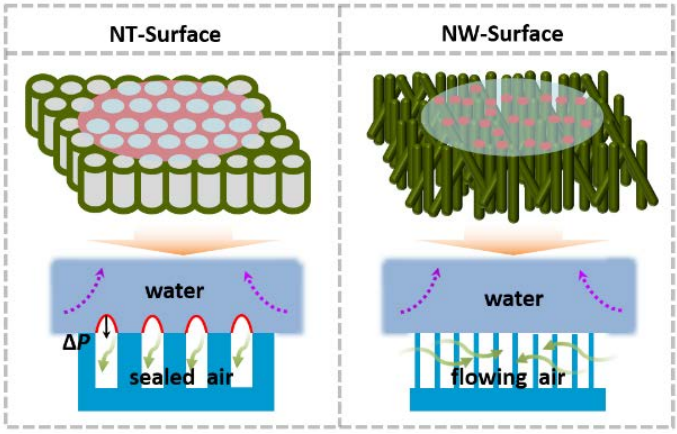

Figure caption list

Figure 1. Schematic illustrations of contact ways between droplets and three superhydrophobic surfaces. (a-d) The contact interfaces of droplets to substrate, NT-Surface, NM-Surface, and NW-Surface, respectively. (e) Bouncing dynamic schematic diagram of impact droplets on the nanostructure-designed surfaces. (f) Diagram on the moving process of impact droplets on solid surfaces containing spreading (at advancing angle θ_A) and retracting processes (at receding angle θ_R).

Figure 2. (a-c) The scanning electron microscope (SEM) images of as-prepared NT-Surface, NM-Surface, and NW-Surface, respectively, and the insets are the images of static droplets suspending on the corresponding nanostructure surface; (d-f) The X-Ray diffraction (XRD) patterns of the corresponding nanostructures. 1, 2, 3, and 4 in Figure (f) represent substrate, after hydrothermal treatment, after acid pickling, and after annealing, respectively; (g) The X-ray photoelectron spectroscopy (XPS) spectrum of the as-prepared TiO_2 nanostructures before and after modifying with low energy groups; (h,i) The testing results on water repellency of the superhydrophobic TiO_2 nanostructure surfaces with APCA and SA.

Figure 3. The contact processes of water droplets impacting on (impact velocity of ~1 m/s, the droplet diameter of 2 mm) Substrate, NT-Surface, NM-Surface and NW-Surface, respectively. We can find that the impact droplet cannot bounce off the NT-Surface, although the surface possesses a higher superhydrophobicity than the untreated substrate surface (unit: ms). The NM-Surface and NW-Surface can both compel the impact droplets to successfully bounce off the surface, yet some differences can be seen that the impact droplet on the NM-Surface shows the loath detachment in comparison to that on the NW-Surface.

Figure 4. (a) Variation of wetting position of water droplets impacting on the nanostructured surfaces with the time, and the wetting position is represented by the value of D/D_0 (D is the diameter of contact area of impact droplet with solid surface, and $D_0 \approx 2$ mm is the initial diameter of droplet). (b) Rate of D/D_0 as a function of time, indicating the detailed distinctions of retracting processes of impact droplets on these sample surfaces. (c) Representative images selected from the retracting processes (at 5.8 ms). (d,e) Interface schematic diagrams of the retracting droplet on NT-Surface and NW-Surface, respectively, and the red area represents the actual solid/liquid contact area. (f,g) Cross section details corresponding to the retracting droplet on NT-Surface and NW-Surface, respectively. Comparing with NW-Surface, NT-Surface can entrap the sealed air pockets underneath the droplets, finally inducing the formation of a negative pressure action (Δf) to prevent the droplet from bouncing off the surface.

Figure

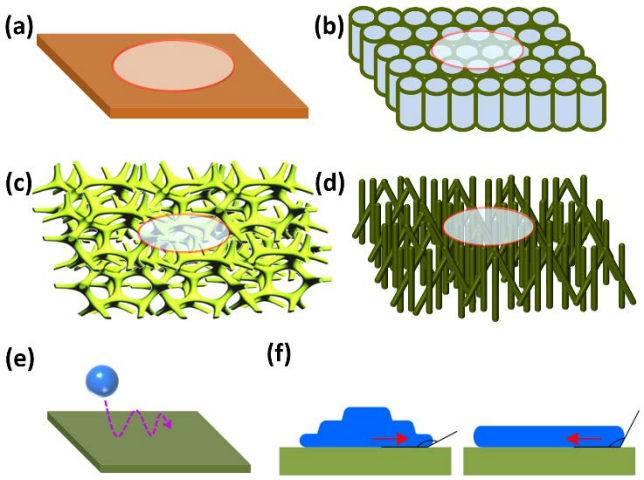

Figure 1. Schematic illustrations of contact ways between droplets and three superhydrophobic surfaces. (a-d) The contact interfaces of droplets to substrate, NT-Surface, NM-Surface, and NW-Surface, respectively. (e) Bouncing dynamic schematic diagram of impact droplets on the nanostructure-designed surfaces. (f) Diagram on the moving process of impact droplets on solid surfaces containing spreading and retracting processes at the dynamic contact angle.

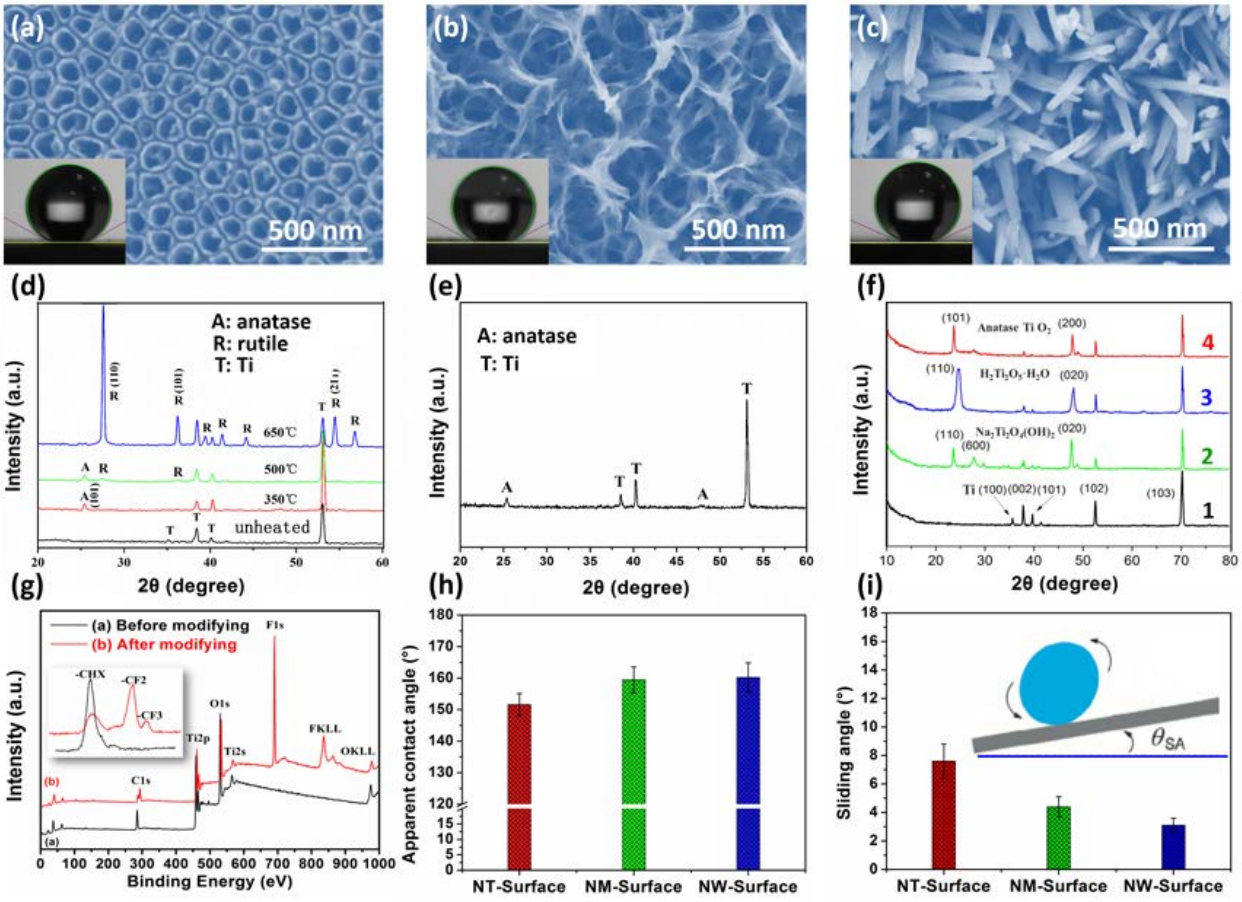

Figure 2. (a-c) The scanning electron microscope (SEM) images of as-prepared NT-Surface, NM-Surface, and NW-Surface, respectively, and the insets are the images of static droplets suspending on the corresponding nanostructure surface; (d-f) The X-Ray diffraction (XRD) patterns of the corresponding nanostructures. 1, 2, 3, and 4 in Figure (f) represent substrate, after hydrothermal treatment, after acid pickling, and after annealing, respectively; (g) The X-ray photoelectron spectroscopy (XPS) spectrum of the as-prepared TiO_2 nanostructures before and after modifying with low energy groups; (h,i) The testing results on water repellency of the superhydrophobic TiO_2 nanostructure surfaces with APCA and SA.

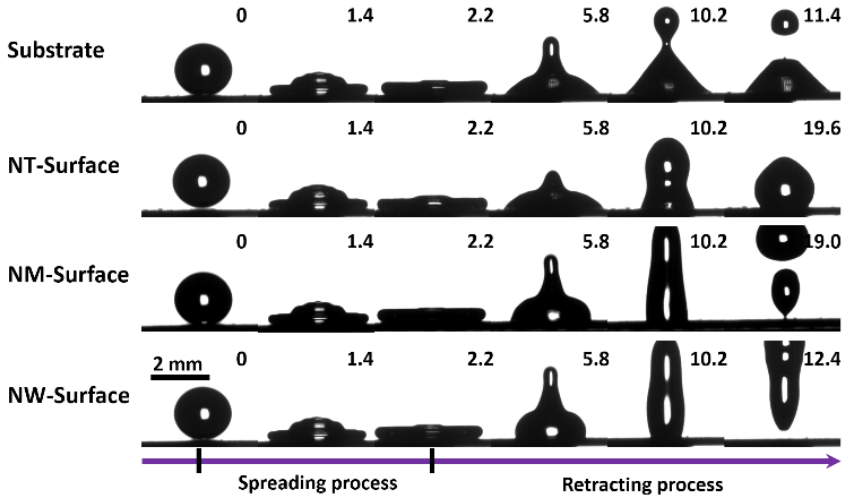

Figure 3. The contact processes of water droplets impacting on (impact velocity of ~1 m/s, the droplet diameter of 2 mm) Substrate, NT-Surface, NM-Surface and NW-Surface, respectively. We can find that the impact droplet cannot bounce off the NT-Surface, although the surface possesses a higher superhydrophobicity than the untreated substrate surface (unit: ms). The NM-Surface and NW-Surface can both compel the impact droplets to successfully bounce off the surface, yet some differences can be seen that the impact droplet on the NM-Surface shows the loath detachment in comparison to that on the NW-Surface.

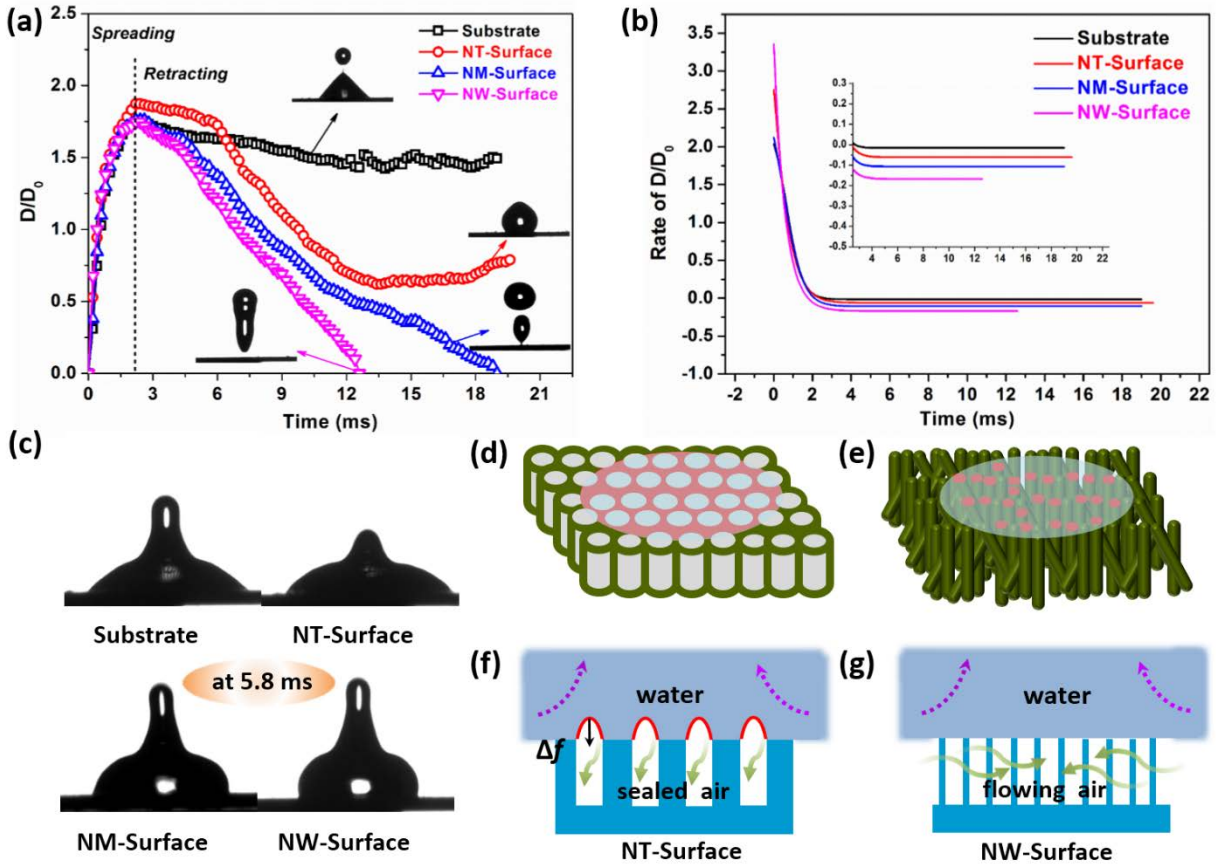

Figure 4. (a) Variation of wetting position of water droplets impacting on the nanostructured surfaces with the time, and the wetting position is represented by the value of D/D_0 (D is the diameter of contact area of impact droplet with solid surface, and $D_0 \approx 2$ mm is the initial diameter of droplet). (b) Rate of D/D_0 as a function of time, indicating the detailed distinctions of retracting processes of impact droplets on these sample surfaces. (c) Representative images selected from the retracting processes (at 5.8 ms). (d,e) Interface schematic diagrams of the retracting droplet on NT-Surface and NW-Surface, respectively, and the red area represents the actual solid/liquid contact area. (f,g) Cross section details corresponding to the retracting droplet on NT-Surface and NW-Surface, respectively. Comparing with NW-Surface, NT-Surface can entrap the sealed air pockets underneath the droplets, finally inducing the formation of a negative pressure action (Δf) to prevent the droplet from bouncing off the surface.